Changes in morphological characteristics of drainage basins following coseismic landslides by the 2018 Hokkaido Eastern Iburi Earthquake

Tennyson Lap Wing LO[1], Yuichi S. HAYAKAWA[2], Yasutaka NAKATA[3], Masato HAYAMIZU[4], Takuro OGURA[5]

[1] Graduate student, Graduate School of Environmental Science, Hokkaido University, Japan

[2] Faculty of Environmental Earth Science, Hokkaido University, Japan

[3] Graduate School of Life and Environmental Sciences, Kyoto Prefectural University, Japan

[4] Forestry Research Institute, Hokkaido Research Organization, Bibai, Japan

[5] Graduate School of Education, Hyogo University of Teacher Education, Japan

連絡責任者：早川裕弌

〒060-0810　札幌市北区北 10 西 5

北海道大学大学院地球環境科学研究院

電話：011-706-2222 FAX：011-706-2222

E-mail: hayakawa@eis.hokudai.ac.jp

Abstract

The 2018 Hokkaido Eastern Iburi Earthquake (Mj 6.7) caused numerous coseismic landslides (n = 7837) covering over 700 km^2. This study aims to identify the post-earthquake morphological changes in drainage basins affected by the landslides, with particular interests in fluvial and slope processes. The study site is a catchment along the Atsuma River with less artificial modifications after the earthquake. Elevation Models (DEMs) of October 2012 and September 2018 with multi-temporal DEMs and orthorectified images in April to October 2020 were used, by which drainage basin morphology, channel network extraction, drainage patterns, stream profile analysis, gullies, morphological change detection and morphometric parameter analysis were conducted. Geomorphometric analysis was performed using Geographical Information System (GIS) to characterize the post-earthquake morphological changes including watershed geometry, channel networks, drainage texture, reliefs, and stream profiles. We infer that, based on the increase in stream length and bifurcation ratio, channels on bare slope surfaces developed progressively and potentially higher surface runoff is expected. With the interactions between fluvial and slope processes, as well as the assists by freeze-thaw actions on bare

soil surfaces, further soil erosion and slope deformations are expected.

Key words: 2018 Hokkaido Eastern Iburi Earthquake, Drainage basin, Morphological changes, Coseismic landslides.

I. Introduction

An intense earthquake can cause drastic slope deformations by coseismic landslides, while continuous changes in slopes, fluvial channels, and drainage patterns are also expected during post-earthquake periods. High-magnitude earthquakes and related coseismic landslides often generate large volumes of mobile sediment in catchments (Keefer, 1984; Keefer, 1994; Wang et al., 2015), which was expected as a key role in the long-term erosional budget (Keefer, 1994; Parker et al., 2011; Roback et al., 2018). Spatial distribution of coseismic landslides are directly related to the distribution of landslide debris, especially coarser ones, in connected channels (Li et al., 2015), and its connectivity for a long term should be related to the catchment-wide geomorphological dynamics including sediment cascades. Therefore, investigation on the sediment connectivity between landslides and channels is crucial for assessing the increase or decrease in the sediment yield in the catchments for decadal or century scales (Koi et al., 2008; Li et al., 2015).

The 2018 Hokkaido Eastern Iburi Earthquake (Mj 6.7) (Japan Meteorological Agency 2019a) caused numerous coseismic landslides (n = 7837) covering over 700 km^2 (Wang et al., 2019), for which the Tarumae-d tephra layer with fine-grained texture and high water infiltration capacity was considered as the inherent factor (Kokusho and Fujita, 2001; Kasai and Yamada, 2019; Ishimaru et al., 2020). Numerous investigations have been carried out for the mechanisms of coseismic landslides in Eastern Iburi region (e.g., Ishimaru et al., 2019; Ishimaru et al., 2020; Kasai and Yamada, 2019; Mizugaki et al., 2019; Wang et al., 2019), but assessments of long-term, post-earthquake changes in drainage basin characteristics including slope and fluvial processes are relatively limited. Even gradual, such post-earthquake changes may cause increase in sediment yield with different patterns (Li et al., 2015; Mizugaki et al., 2019), and it is necessary to continuously monitor the post-earthquake changes in slope and fluvial characteristics in the Iburi region.

The present research aims to assess the changes in morphological characteristics of drainage basins following the coseismic landslides by the 2018 Hokkaido Eastern Iburi Earthquake, and explore slope and fluvial processes affecting the morphological changes.

II. Study Area

A large amount of coseismic landslides were formed around Atsuma and Abira Towns in southern Hokkaido with the 2018 Hokkaido Eastern Iburi Earthquake at 03:07 am on September 6th (Japan Meteorological Agency 2019a), whose epicenter was at 42.690°N and 142.007°E with the focus depth of 37 km (Japan Meteorological Agency 2019). The eastern Iburi region is an area with folding and faulting (Ayalew et al., 2011), and the major bedrock is Neogene Sedimentary rocks (23 – 2.6 Ma) with weakly consolidated materials (Matsuno and Ishida, 1960; Takahashi et al., 1984). The land surface is blanketed by thick (1–3 m) tephra layers of volcanic pumice (Uda et al., 1979; Hirose et al., 2018; Yamagishi and Yamazaki., 2018). There are three major types of the tephra layers, namely Sikotsu pumice fall (Spfa-1, 42 ka) by the Shikotsu caldera eruption (Machida and Arai, 2003), Eniwa pumice fall (En-a, 20 ka) by the Eniwa volcano eruption (Machida and Arai, 2003) , and Tarumae pumice fall (Ta-d, 9 ka) by the Tarumae volcano eruption (Furukawa and Nakagawa, 2010; Hirose et al.,2018; Ishimaru et al., 2020). The En-a layer with a thickness of more than 100 cm predominantly covers the northern part of the landslide-affected area, while the Ta-d layer with more than 50 cm thickness covers the southern part. These tephra layers are considered as the main constituents of the coseismic landslides (Ishimaru et al., 2020), because the fine-grained (0.008 – 0.71 mm) tephra layer is supposed to be sensitive to the liquefaction contributing to slope failure (Kokusho and Fujita, 2001; Petley, 2018; Kasai and Yamada, 2019).

The study site is an approximately 0.1 km^2 watershed, a tributary of the upper reach of the Atsuma River located at about 10 km from the epicenter (Figure 1). A large fraction of slopes (approximately 20%) in the watershed are affected by the coseismic landslides. In this area, because no residential houses are present, relatively less impacts by artificial modification are expected after the earthquake. However, small check dams have been constructed at the outlet of the tributaries draining into the downstream Apporo Reservoir. According to the Atsuma Meteorological Station (42°43.8’N, 141°53.3’E, ca. 11 km to the west away from the study site), the annual mean temperatures were 3.4°C, 4.7°C, 4.7°C for 2018, 2019 and 2020 respectively. The annual maximum and minimum temperatures were 30.9°C and -24.1°C (2018), 32.2°C and -22.9°C (2019), and 32.9°C and -23.6°C (2020) (Japan Meteorological Agency, 2023). Maximum snow depth in the region is 70 cm in average (1991-2020) peaking in February, according to the nearby meteorological station at Abira (42°48.8´N, 141°44.7´E, ca. 15 km away) (Japan Meteorological Agency, 2023).

Fig. 1

III. Data Collection and Analysis

1. Data Collection

Digital elevation models (DEMs) with a 0.5-m resolution, generated from airborne laser scanning (ALS) data of October 5 in 2012 and September 11 in 2018 (Hokkaido Prefecture, 2020a, b), were used to represent the topography of pre- and post-earthquake. Acquisition of aerial photos by unmanned aerial vehicle (UAV) were conducted in the field for four times from April to October in 2020 (April 23, June 25, September 14, and October 30). A UAV of DJI Phantom 4 RTK, equipped with an RGB camera (20 M sensor and pre-calibrated lens), was used with the terrain following mode to keep the relative flight height of 100 m from the ground. A base station of global navigation satellite system (GNSS) receiver (DJI D-RTK2) was used to perform the real-time kinematic (RTK) correction of the GNSS-derived aircraft positions during the flight, providing the geographic coordinates of each camera image at a centimeter-level accuracy. Based on the UAV-based aerial images, Structure-from-Motion Multi-View Stereo (SfM-MVS) photogrammetry (Hayakawa and Obanawa, 2016; Hayakawa et al., 2016) was then performed using Agisoft Metashape software to generate point cloud, DEMs, and orthorectified mosaic images. The resolution of DEMs and orthorectified images were set at the finest capability (several to ten centimeters) of the SfM-MVS photogrammetry for each dataset (Table 1).

The period of available datasets was divided into five sections as follows (Table 1). Period 1: from October 2012 to September 2018 (6 years including the earthquake event), for which ALS DEMs are available; Period 2: September 2018 to April 2020 (approximately 1.5 years), for which ALS- and UAV-derived DEMs are applied; Period 3: April 23 to June 25 (2 months), Period 4: June 25 to September 14 (3 months); and Period 5: September 14 to October 30 (1.5 month) in 2020. UAV-derived data are available for Periods 3 to 5.

Table 1

According to the Atsuma Meteorological Station (42°43.8’N, 141°53.3’E, ca. 11 km west away from the study site), total annual rainfall in Atsuma region was 1136.5 mm in 2018, 849.0 mm in 2019, and 797.5 mm in 2020 (Japan Meteorological Agency, 2018, 2019b and 2020). In 2018, Typhoon No. 21 on September 5 with a maximum rainfall intensity of 9 mm/hr and total rainfall of 12 mm. Typhoon No. 24 which on October 1, 2018 with a maximum rainfall intensity of 9.5 mm/hr and 13.5 mm/hr on October 1 and 2, respectively (Japan Meteorological Agency, 2018). The rainfall intensity increased gradually from April 25, 2019 to Oct 4, 2019 with highest 19.5 mm/hr rainfall intensity due to the intensive rainfall by Typhoon No. 18 which approached Hokkaido on October 4, 2019 (Japan Meteorological Agency, 2019b). Also, 13.5 mm/hr and 16.5 mm/hr rainfall intensity were also recorded in Period 4 while only a low intensity of 7 mm/hr was observed during the Period 5 (Figure 2) (Japan Meteorological Agency, 2020). Number of days with maximum temperature above 0°C and minimum temperature below 0°C in each month from December 2018 to May 2020 at Atsuma Meteorological Station are shown in Figure 3. These data may be the reference for indicating correspondence of morphological changes on the landslide-affected slopes with freezing and thawing.

Fig. 2

Fig. 3

2. Geospatial Analysis

Geographic Information System (GIS) software QGIS 3.22.7 was used for geospatial analysis of the topographic data. Hydrological and geomorphometric analyses were performed to characterize the morphological properties of the watershed, streams, and reliefs in the catchment, and the changes in elevation. For the extraction of streams, we set a threshold value of 100 m^2 as the channel heads which visually corresponds to the morphological features of channel heads.

For geomorphometric analysis, ten main parameters, which are categorized into three types of drainage network, drainage texture, and relief characteristics, were derived from the DEM and stream network data to analyze temporal changes in drainage basin characteristics (Table 2). Ten parameters are selected because they may indicate the form and predominant processes within watershed relating to mass movement, surface water and understanding of soil erosion and discharge characteristics of ungauged stream (Prabhakaran et al., 2018). Stream number (N_u) is the number of stream segments within watershed (Horton 1945). Stream length (L_u) is the horizontal distance of channel from the stream head to the stream outlet (Horton, 1945; Strahler, 1964). Bifurcation ration (R_b) is measuring the ratio of the number of streams of a given stream order to the number of streams of next higher order (Horton, 1945; Strahler, 1964) to indicate the amount of branching in the stream network within a watershed (Doornkamp and King, 1971). Mean gradient of mainstream (m/m) is the ratio of difference in maximum and minimum elevation of mainstream to the horizontal distance of stream channel between stream head and stream outlet. Drainage density (D_d) refers to the total length of streams within a watershed per unit area (Horton, 1932) which is one of the most sensitive and variable morphometric parameters with direct relationship with rainfall intensity (Chorley and Morgan, 1962), mean annual runoff (Morisawa, 1962), and an inverse relationship with the degree of development of a drainage net within a basin (Horton, 1945), and texture of landscape dissection and spacing of streams (Chorley, 1969). Drainage intensity (D_i) was defined as the ratio of the stream frequency to the drainage density (Faniran, 1968). Infiltration number (I_f) reflects the infiltration potential of a watershed (Faniran, 1968) and lower infiltration numbers may imply higher infiltration and less surface run-off (Faniran, 1968; Das and Mukherjee, 2005; Joji et al., 2013; Elewa et al., 2016). Length of overland flow (L_o) can describe the length of flow of water over the ground surface before it becomes concentrated in definite stream channels (Horton, 1945). In watersheds with shorter length of overland flow values, rain water will enter the stream relatively quickly, and lesser rainfall is sufficient to contribute a significant volume of surface run off to stream discharge (Prabhakaran et al., 2018). The constant of channel maintenance (C) was suggested by Schumm (1956) to indicate the number of km^2 of basin surface required to develop and sustain a channel 1 km long. Ruggedness number (R_n) is an index suggested by Strahler (1964) which can reflect the situation of slope steepness and length in a watershed. High values of the ruggedness number indicated that slopes are steep and long (Chow, 1964) which may affect the velocity, infiltration and discharge in watershed.

IV. Results

1. Coseismic Morphological Changes (Period 1)

The 2012 ALS DEM illustrates the situation of drainage basin before the 2018 Hokkaido Eastern Iburi Earthquake (Figure 4a), while the 2018 ALS DEM shows the situation after the earthquake (Figure 4b). By comparing these two DEMs, considerable areas (ca. 21,000 m^2 within the catchment area of 70,000 m^2) are affected by the coseismic landslides from the middle to upper part of the drainage basin. Also, sediment deposition is noticeably observed along the lower reach of the mainstream.

The total stream length in 2012 was 721.3 m with mean gradient of mainstream 0.17 m/m (Table 3), where 5 tributaries were identified (Figure 4c). The total stream length in 2018 was 932.9 m with mean gradient of mainstream 0.12 m/m (Table 3) with 10 tributaries (Figure 4d). The total stream length in 2018 was 211.6 m longer and mean

Table 2

Fig. 4

gradient of mainstream in 2018 was 0.05 lower than that of 2012 respectively.

2. Post-earthquake Morphological Changes (Periods 2-5)

Figures 5 and 6 show the stream network and longitudinal profiles, respectively, derived from the DEMs in 2020. From September 2018 to April 2020 (Period 2), due to the repairment of the road and construction of a check dam at the outlet, the sediment was partially removed, and the affected 50 m reach was excluded in the following analysis of the mainstream. The mainstream channel length decreased to 516.0 m, which was 137.8 m shorter than in 2018, while eight tributaries were identified. The total stream length was 753.9 m in April 2020, which was 179.1 m shorter than in 2018. The mean stream gradient was 0.15 m/m, which was steeper than in 2018.

From April to June 2020 (Period 3), the mainstream channel length further decreased to 498.2 m (17.8 m shorter), and the mean gradient increased to 0.17 m/m. Seven tributaries were identified. The total stream length was 694.3 m, which was 59.6 shorter than in April.

Fig.5 & 6

From June to September 2020 (Period 4), the mainstream channel length increased to 564.9 m (66.7 m longer), while the mean gradient also increased to 0.21 m/m. Nineteen tributaries were identified and the total stream length was 1121.9 m, which was 427.6 m longer than in June.

From September to October (Period 5), the mainstream channel length increased to 595.0 m (30.1 m longer), while the mean gradient also decreased to 0.14 m/m. Nineteen tributaries were identified and the total stream length was 1199.6 m, which was 77.7 m longer than in September.

3. Temporal Changes in Morphometric Parameters

Morphometric parameters representing drainage network, drainage texture, and relief characteristics for each dataset were summarized in

Table 3

Table 3.

Regarding parameters of drainage network, the stream number (*N*u) increased from 6 to 11 after the earthquake. After the slight decreasing to 8 in June 2020, it increased to 22 in September 2020 and slightly decreased to 20 in October 2020. The total stream length increased from 721.3 m to 932.9 m after the earthquake and finally increased to 1121.9 m in the post-earthquake period 4. The bifurcation ratio increased from 5 to 10 and it kept rather constantly high (7–9.5) in the post-earthquake periods 3 and 4, and reached the highest value of 19 in period 5.

For drainage texture, there was an increasing trend in drainage density from 6.94 to 11.53, drainage intensity from 8.32 to 19.61, infiltration number from 400.57 to 2217.92 throughout all the periods. In contrast, the length of overland flow (from 0.07 to 0.04) and constant of channel maintenance (from 0.14 to 0.09) showed decreasing trend.

As relief characteristics, ruggedness number increased from 1.18 to 1.81 throughout the periods.

By comparing the results after the earthquake, the results of the stream number, total stream length, bifurcation ratio, drainage density, intensity, infiltration number decreased in Periods 2 and 3, and some of them with their lowest values in Period 3. In contrast, the length of overland flow and constant of channel maintenance had an increasing trend and increased to their highest values in Period 3.

V. Discussion

The morphological changes of the drainage basin characteristics by the earthquake are apparently associated with the slope modifications by the coseismic landslides. Whereas, morphological changes and fluvial network development in drainage basin after the earthquake might correspond to gradual or periodical erosion by fluvial and/or slope processes associated with cold climate. One possible reason for the variable changes in the morphological parameters in the post-earthquake periods is the hydrological variability in fluvial processes that likely forms the gully and channel networks on the bare surface of the landslide areas, and the temporal distribution of rainfall intensity (Figure 2) can be the main factor for the morphological change variability. The amount and pattern of rainfall intensity during post-earthquake periods might play an important role in the changes of drainage basin morphology and stream network development in the study site. Some Typhoon-induced rainfalls were present in Period 2 (Typhoon No. 24 in October 2018 and Typhoon No. 18 in October 2019), but there were no Typhoon attacks in the following periods (Periods 3-5; Figure 2). However, relatively high rainfall intensity was also recorded in post-earthquake Period 3 (11.5 mm/hr), Period 4 (16.5 mm/hr), and Period 5 (7 mm/hr). Relatively strong increase in stream length, drainage density, drainage intensity and infiltration number in Period 4 may correspond to the high-intensity rainfall event, which potentially contributed to the gully development on the bare slope surfaces by increased runoff. In fact, significant gully erosion was observed on landslide-affected slopes in northwestern Atsuma town with similar conditions to our study area during the rainy seasons from June to August in 2019 and from May to October in 2020 (Koshimizu et al., 2021). Those changes may also have occurred during Period 2, but this might be hindered by the longer time period (nearly 2 years) compared to the other periods (2–3 months) due to the infilling processes after erosion (Imaizumi et al., 2010).

Freeze-thaw weathering and solifluction by periodical fluctuation of temperature around the freezing point (Matsuoka and Murton, 2008; Deprez, et. al., 2020) could also contribute to the enhancement of the infilling process on gully and channel thalwegs. Such a process has been particularly active in the last glacial period (~10 ka) in Hokkaido

(Ishimaru et al., 2020), while it also influences the soil surface for more than 10 cm to cause mass movements of surface materials on the vegetation-free slopes in the modern time (Ueno et al., 2015; Nakata et al., 2021). In fact, up to 5 cm topographic changes resulting from freeze-thaw action was observed based on differential analysis of DEMs in daytime and nighttime on a slope in coseismic landslide area in Takaoka, near our study site (Nakata et al., 2021).Number of days with maximum temperature above 0°C and minimum temperature below 0°C in each month in the region (Figure 3) indicates the possible frequent occurrences of freeze-thaw actions on the bare slope surfaces in the study area especially in the autumn and spring seasons (Figure 7). Although the actual soil surface temperature in the study site is unknown, such a condition favorable for freeze-thaw actions may be associated with the rapid infilling of gullies after the Typhoon attacks during Period 2.

Figure 7

The gradual changes in main channel length and gradient of main channel especially during the post-earthquake period 4-5 indicated some slope movement on slid surfaces with morphological changes and fluvial erosion on gully stream channels. The increase in drainage density (D_d) might imply more rapid surface runoff and shorter lag time with higher peak on hydrograph (Chorley, 1969). The higher the value of drainage intensity (D_i) might indicate higher rate of gully erosion. The higher the infiltration number (I_f), the lower will be the infiltration and as a result, the higher surface run-off might be expected (Faniran, 1968). The decrease in length of overland flow (L_o) which indicate larger volume of surface runoff to stream discharge might contribute to the fluvial erosion along streams. Moreover, the increase in drainage density might cause the decrease in constant of channel maintenance (C) which implies more tributaries. Finally, the increasing trend on gradient might imply higher risk of slides on slope with increased surface runoff and stream discharge.

VI. Conclusions

Regarding the coseismic landslides by the 2018 Hokkaido Eastern Iburi Earthquake, we examined the morphological changes in a landslide-affected catchment for periods between pre- and post-earthquake, and of post-earthquake, and quantified the areas of coseismic landslides, continuous sediment deposition and changes in drainage basin characteristics were identified. The results also suggest continuous changes in drainage networks after the earthquake, which may largely depend on the rainfall intensity and associated fluvial erosion, as well as slope surface modifications by freeze-thaw actions. The sedimentation in downstream areas and continuous fluvial erosion on surrounding slid slopes might changes in the form of watershed with elevation increase and decrease in lower and upper parts of watershed respectively.

This study provides an inventory of drainage basin morphological changes and drainage network development after the 2018 Hokkaido Eastern Iburi Earthquake. Analyzed results should be further validated in monitoring of post-earthquake landslides. Future work may focus on the near-future fluvial landscape evolutionary studies, and it would also be beneficial for the investigation of sediment connectivity in the region.

Acknowledgements

We thank Mio Kasai, Takayuki Shiraiwa, Maiku Abe, and Teiji Watanabe for their generous supports on field surveys, data analysis, and constructive discussion. This study is partly supported by Hokkaido University DX fellowship Grant, Hokkaido University Support System for the Joint Research of Next-Generation Researchers, and JSPS KAKENHI Grant Numbers JP16KK0012, JP17H02031, JP21H00625, JP18H03957, JP18H02235, JP19K01156, JP21H00627, and JP22H02374.

References

Ayalew, L., Kasahara, M. and Yamagishi, H. (2011): The spatial correlation between earthquakes and landslides in Hokkaido (Japan), a GIS-based analysis of the past and the future. *Landslides*. 8(4):433–448.

Chow, V.T. (1964): Handbook of Applied Hydrology. *McGraw-Hill Book Company, New York.*

Chorley, R.J. and Morgan, M.A. (1962): Comparison of morphometric features, Unaka Mountains, Tennessee and North Carolina, and Dartmoor, England. *Geological Society of America Bulletin*, 73, 17 – 34.

Chorley, R.J. (1969): Introduction to physical hydrology. *Methuen and Co., Ltd., Suffolk.* 211.

Das, A.K. and Mukherjee, S. (2005): Drainage Morphometry Using Satellite Data and GIS in Raigad District, Maharashtra. Engineering, Environmental Science Journal of Geological Society of India. 65, 577-586.

Deprez, M., Kock, T. D., Schutter, G. D and Cnudde. V. (2020): The role of ink-bottle pores in freeze-thaw damage of oolithic limestone. *Construction and Building Materials*, 246 (118515), 1-12. 10.1016/j.conbuildmat.2020.118515

Doornkamp, J. C., King, CAM. (1971): Numerical analysis in geomorphology—an introduction. *Macmillan and Co. Ltd, London*. 372.

Elewa, H.H., Ramadan, E.M. and Nosair, A.M. (2016): Spatial-based hydro-morphometric watershed modeling for the assessment of flooding potentialities. *Environmental Earth Scienc*e. 75, 906–927. https ://doi.org/10.1007/s1266 5-016-5692-4

Faniran, A. (1968): The index of drainage intensity—a provisional new drainage factor. *Australian journal of science*, 31, 328–330.

Furukawa, R. and Nakagawa, M. (2010). Geological Map of Tarumae Volcano. Geological Map of Volcanoes 15. *Geological Survey of Japan*, AIST, 1–7.

Hayakawa, Y. S., Obanawa, H., Saito, H. and Uchiyama, S. (2016): Geomorphological Applications of Structure-from-Motion Multi-View Stereo Photogrammetry: A Review. *Transactions, Japanese Geomorphological Union*, 37-3, 321-343.

Hayakawa, Y. S. and Obanawa, H. (2016): Aerial measurements of topography using small UAS and SfM-MVS photogrammetry. *Butsuri-Tansa (Geophysical Exploration)*, 69 (4), 297-309. (in Japanese with English abstract)

Hirose, W., Kawakami, G., Kase, Y., Ishimaru, S., Koshimizu, K., Koyasu, H. and Takahashi, R. (2018): Preliminary report of slope movements at Atsuma Town and its surrounding areas caused by the 2018 Hokkaido eastern Iburi earthquake. *Reports of the Geological Survey* *of Hokkaido*, 90, 33–44 [in Japanese].

Hokkaido Prefecture (2020a): Hokkaido airborne laser scanning data 2018 Atsuma. https://www.harp.lg.jp/opendata/dataset/1401.html (in Japanese) [Last accessed: 2021.12.01]

Hokkaido Prefecture (2020b): Hokkaido airborne laser scanning data 2012 Atsuma Reservoir. https://www.geospatial.jp/ckan/dataset/h24atumadamu-kensetukouji (in Japanese) [Last accessed: 2021.12.01]

Horton, R.E. (1932): Drainage basin characteristics. *Transactions American Geophysical Union*, 13, 350－361

Horton, R. E. (1945): Erosional development of stream and their drainage basins; hydrophysical approach to quantitative morphology. *GSA Bulletin*, 56 (3): 275–370.

Imaizumi, F., Hattanji, T. and Hayakawa, Y. S. (2010): Channel initiation by surface and subsurface flows in a steep catchment of the Akaishi Mountains, Japan. *Geomorphology*, 115, 32–42. www.elsevier.com/locate/geomorph

Ishimaru, S., Hirose, W., Kawakami, G., Takahashi, R., Kase, Z., Koshimizu, K., Koyasu, H., Chigira, M. and Tajika, J. (2019): The sources of landslides occurred by the 2018 Hokkaido Eastern Iburi Earthquake. *Abstracts, Japan Geoscience Union Meeting 2019*, HDS14-01.

Ishimaru, S., Hirose, W., Kawakami, G., Koshimizu, K., Koyasu, H., Kase, Y., Takahashi, R., Chigira, M. and Tajika, J. (2020): Multiple landslides Caused by the 2018 Hokkaido Eastern lburi Earthquake: Topographic Features of Tephra landslides from the Viewpoint of Geomorphic Development. Transactions, *Japanese Geomorphological Union*, 41 (2), 147-167. (in Japanese with English abstract)

Japan Meteorological Agency (2018): *Historical Weather Data Search*. https://www.data.jma.go.jp/obd/stats/etrn/index.php (in Japanese) [Last accessed: 2023.01.18]

Japan Meteorological Agency (2019a): Earthquake Report during the Disaster of The 2018 Hokkaido Eastern Iburi Earthquake. https://www.jma.go.jp/jma/kishou/books/saigaiji/saigaiji_201901.pdf (in Japanese) [Last accessed: 2023.01.18]

Japan Meteorological Agency (2019b): *Historical Weather Data Search*. https://www.data.jma.go.jp/obd/stats/etrn/index.php (in Japanese) [Last accessed: 2023.01.18]

Japan Meteorological Agency (2020): *Historical Weather Data Search*. https://www.data.jma.go.jp/obd/stats/etrn/index.php (in Japanese) [Last accessed: 2023.01.18]

Japan Meteorological Agency (2023): *Historical Weather Data Search*. https://www.data.jma.go.jp/obd/stats/etrn/index.php (in Japanese) [Last accessed: 2023.01.18]

Joji V.S., Nair, A.S.K. and Baiju, K.V. (2013): Drainage basin delineation and quantitative analysis of Panamaram watershed of Kabani River

Basin, Kerala using remote sensing and GIS. *Journal Geological Society of India*, 82, 368-378.

Kasai, M. and Yamada, T. (2019): Topographic effects on the frequency-size distribution of landslides triggered by the 2018 Hokkaido Eastern Iburi earthquake, Japan. *Geophysical Research Abstracts*, 21, 17656.

Keefer, D. K. (1984): Landslides caused by earthquakes. *Geological Society of America Bulletin*, 95(4), 406-421.

Keefer, D. K. (1994): The importance of earthquake-induced landslides to long-term slope erosion and slope-failure hazards in seismically active regions. *Geomorphology*, 10 (1994), 265-284.

Koi, T., Hotta, N, Ishigaki, I., Matuzaki, N., Uchiyama, Y. and Suzuki, M. (2008): Prolonged impact of earthquake-induced landslides on sediment yield in a mountain watershed: The Tanzawa region, Japan. *Geomorphology*, 101 (4), 692-702. https://doi.org/10.1016/j.geomorph.2008.03.007

Kokusho, T. and Fujita, K. (2001): Water films involved in post-liquefaction flow failure in Niigata City during the 1964 Niigata earth-quake. *Recent Advances in Geotechnical Earthquake Engineering and Soil Dynamics.* 5, 38

Koshimizu, K., Ishimaru, S., Kawakami, G., Nakata, Y., Takami, M and Urabe, A. (2021): Sediment dynamics of an earthquake-induced landslide due to the effects of rainfall and snowmelt: Examination by multi-temporal UAV-SfM survey data. *International Journal of*

Erosion Control Engineering(砂防学会誌), 74(3), 26-36.

Li, G., West, Densmore, A. L., Hammond, D. E., Jin, Z., Zhang, F., Wang, J., Robert G. and Hilton, R. G. (2015): Connectivity of earthquake-triggered landslides with the fluvial network: Implications for landslide sediment transport after the 2008 Wenchuan earthquake. *Journal of Geophysical Research: Earth Surface*, 121 (4), 703-724. https://doi.org/10.1002/2015JF003718

Machida, H. and Arai, F. (2003). Atlas of Tephra in and around Japan, new edn. *University of Tokyo Press.* [in Japanese].

Matsuno, K. and Ishida, M. (1960): Explanatory Text of the Geological Map of Japan Scale 1: 50,000, Hayakita, *Hokkaido Development Agency*. Sapporo, 43. (in Japanese)

Matsuoka, N. and Murton, J. (2008) Frost weathering: recent advances and future directions. *Geology Permafrost and Periglacial Processes*. 19, 195-210, 10.1002, 620.

Mizugaki, S., Murakami, Y. and Fujinami, T. (2019): Suspended sediment discharge from the Atsuma River after the Hokkaido East Iburi Earthquake *Proceeding for the 63th Hokkaido Development Technology Research Meeting*. https://www.hkd.mlit.go.jp/ky/jg/gijyutu/splaat000001t3qf-att/splaat000001t3xi.pdf

Morisawa, M. E. (1962): Quantitative geomorphology of some watersheds in the Appalachian Plateau. *Geological Society of America Bulletin*. 73, 1025-1046.

Nakata, Y., Hayamizu, M., Ishiyama, N. and Torita, H. (2021): Observation of Diurnal Ground Surface Changes Due to Freeze-Thaw Action by Real-Time Kinematic Unmanned Aerial Vehicle. *Remote Sensing*. 13, 11. 2167. https://doi.org/10.3390/rs13112167

Parker, R. N., Densmore, A. L., Rosser, N. J., de Michele, M., Li, Y., and Huang, R. (2011): Mass wasting triggered by the 2008 Wenchuan earthquake is greater than orogenic growth. *Nature Geoscience*, 4(7), 449–452. https://doi.org/10.1038/ngeo1154

Petley, D. (2018): Landslides triggered by the 6th September 2018 Hokkaido earthquake. https://blogs.agu.org/landslideblog/2018/09/06/landslides-6th-september-2018-hokkaido-earthquake/.

Prabhakaran, A. and Jawahar Raj, N. (2018): Drainage morphometric analysis for assessing form and processes of the watersheds of Pachamalai hills and its adjoinings, Central Tamil Nadu, India. *Applied Water Science*, 8, 31.

Roback, K., Clark,M. K., Western, A. J., Zekkos, D., Li, G., Gallen, S.f., Chamlagain, D. and Godt, J. W. (2018): The size, distribution, and mobility of landslides caused by the 2015 Mw7.8 Gorkha earthquake, Nepal. *Geomorphology*, 301, 131-138.

Schumm, S.A. (1956): Evolution of drainage systems and slopes in badlands at Perth Amboy, New Jersey. *Geological Society of America Bulletin*, 67, 597 – 646.

Strahler, AN. (1964): Part II. Quantitative geomorphology of drainage basins and channel networks. *Handbook of Applied Hydrology: McGraw-Hill*, *New York*, 39, 4, 4-7.

Takahashi, K., Fukusawa, H., Wada, N., Hoyanagi, K. and Oka, T. (1984): Neogene stratigraphy and Paleogeography in the Area along the Sea of Japan of northern Hokkaido. *Earth Science (Chilyu Kagaku),* 38, 299-312.

Uda, T., Kimura, G., Aida, Y. and Tonosaki, T. (1979): Active fault crosscut pumice layer of Tarumae pumice fall deposit. *Earth Science*, 33, 304–307, https://doi.org/10.15080/agcjchikyukagaku.33.5_304 [in Japanese].

Ueno, K., Kurobe, K., Imaizumi, F. and Nishii, R. (2015): Effects of deforestation and weather on diurnal frost heave processes on the steep mountain slopes in south central Japan. *Earth Surface Processes and Landforms*, 40, 2013–2025.

Wang, F., Fan, X., Yunus, A. P., Subramanian, S. S., Alonso-Rodriguez, A., Dai, L., Xu, Q. and Huang, R. (2019): Coseismic landslides triggered by the 2018 Hokkaido, Japan (Mw 6.6), earthquake: spatial distribution, controlling factors, and possible failure mechanism. *Landslides*, 16 (8), 1551–1566. https://www.researchgate.net/publication/333306029_Coseismic_landslides_triggered_by_the_2018_Hokkaido_Japan_Mw_66_earthquake_spatial_distribution_controlling_factors_and_possible_failure_mechanism

Wang, J., Jin, Z., Hilton, R. G., Zhang, F., Densmore, A. L., Li, G. and West, A. J. (2015): Controls on fluvial evacuation of sediment from earthquake-triggered landslides. *Geology*, 43 (2), 115-118.

Yamagishi, H. and Yamazaki, F. (2018): Landslides by the 2018 Hokkaido Iburi-Tobu Earthquake on September 6. *Landslides*, 15, 2521–2524, https://doi.org/10. 1007/s10346-018-1092-z

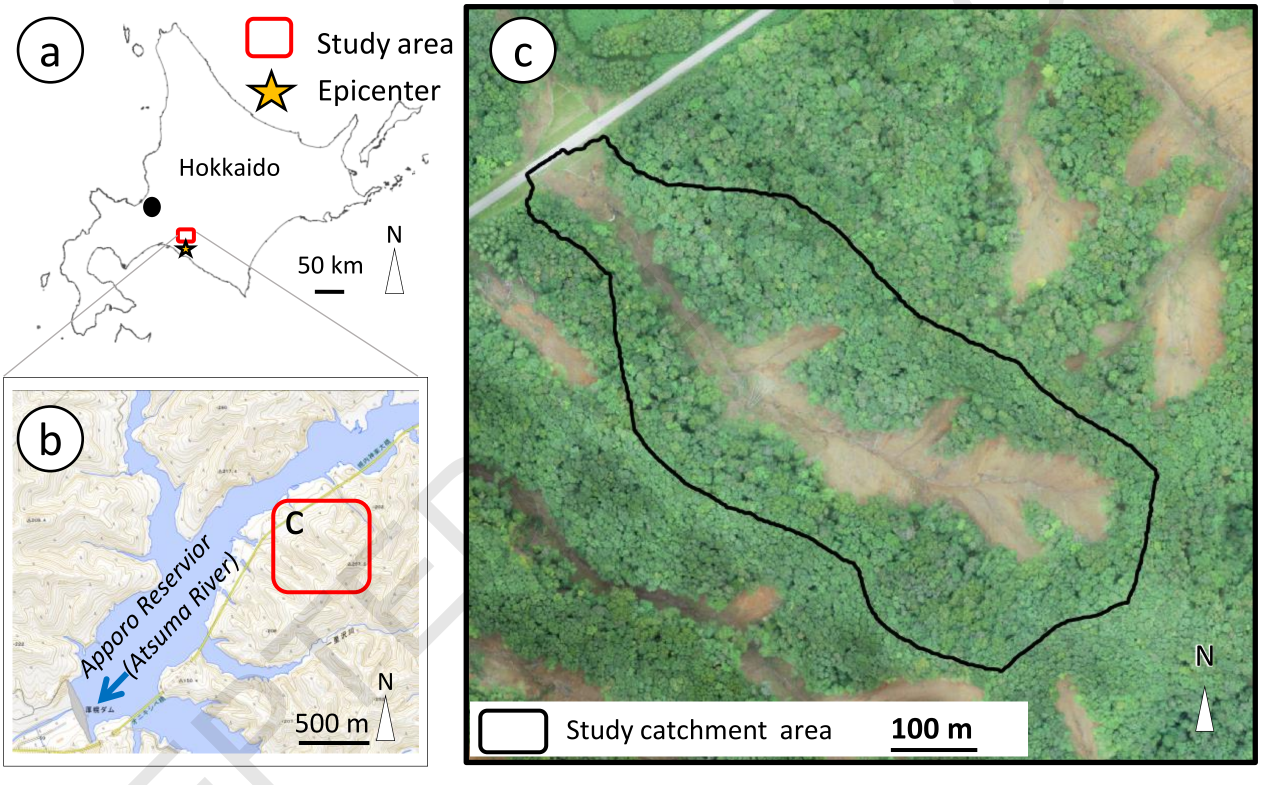

Figure 1. Study area. (a) Overview of the study area (GSI Maps). (b) Topographic maps around the study area (GSI Maps). (c) UAV-based orthorectified image of the catchment studied (14th Sep, 2020).

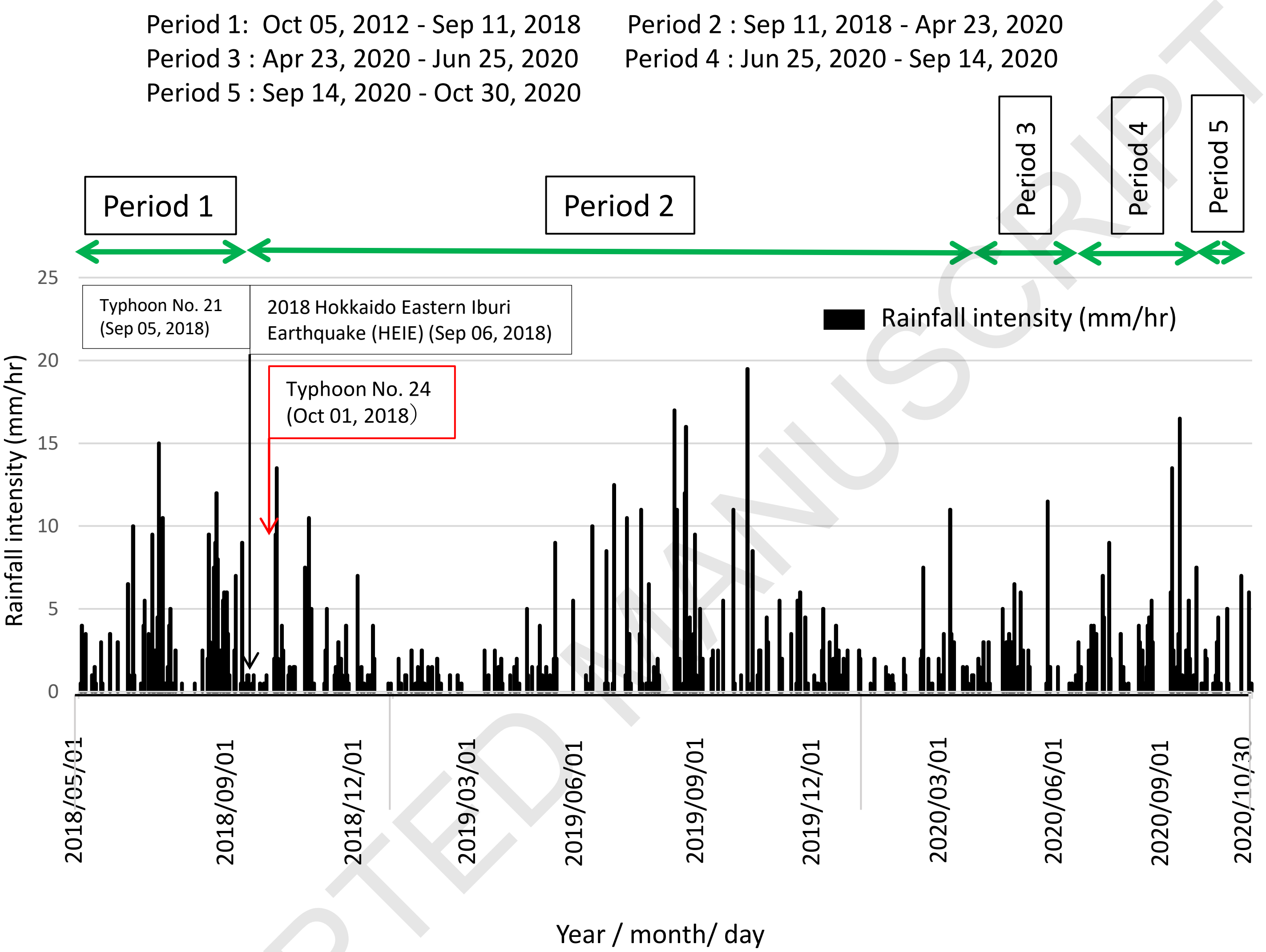

Figure 2. Rainfall intensity (mm/hr, daily maximum) from May 2018 to October 2020 recorded by Atsuma Meteorological Station (Japan Meteorological Agency, 2023)

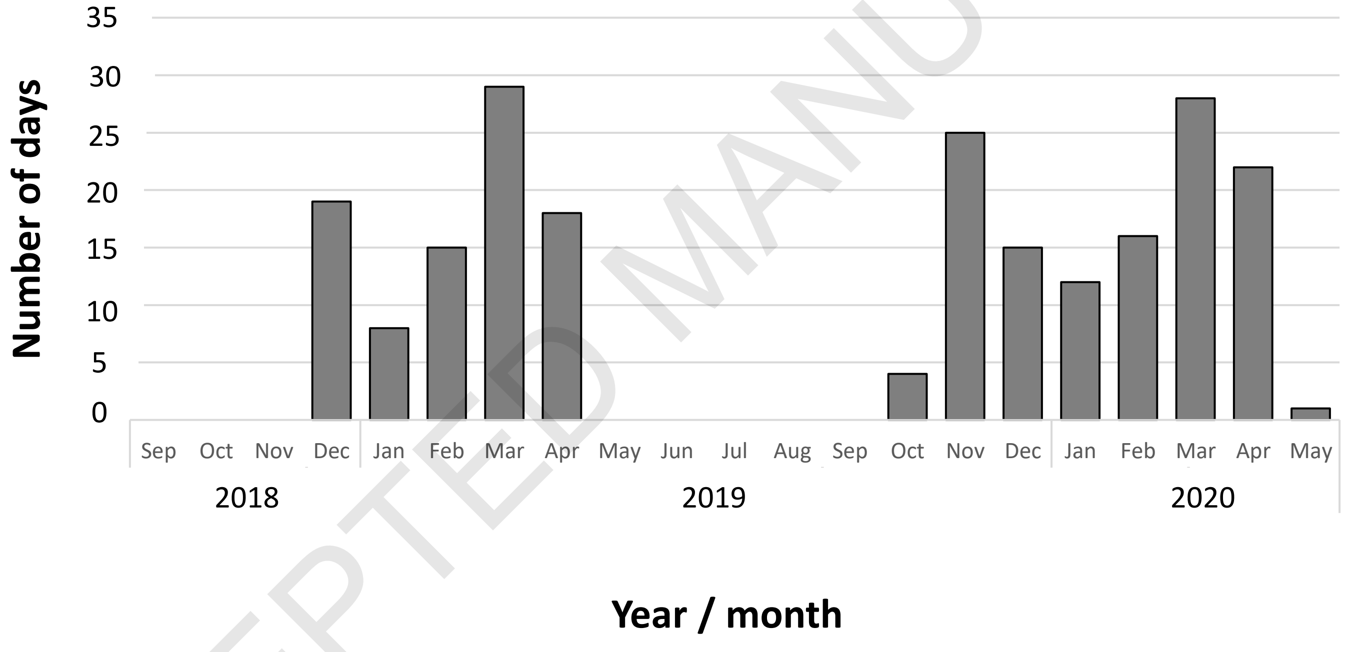

Figure 3. Number of days with maximum and minimum temperature above and below 0°C in each month from September 2018 to May 2020 at Atsuma Meteorological Station (Japan Meteorological Agency, 2020)

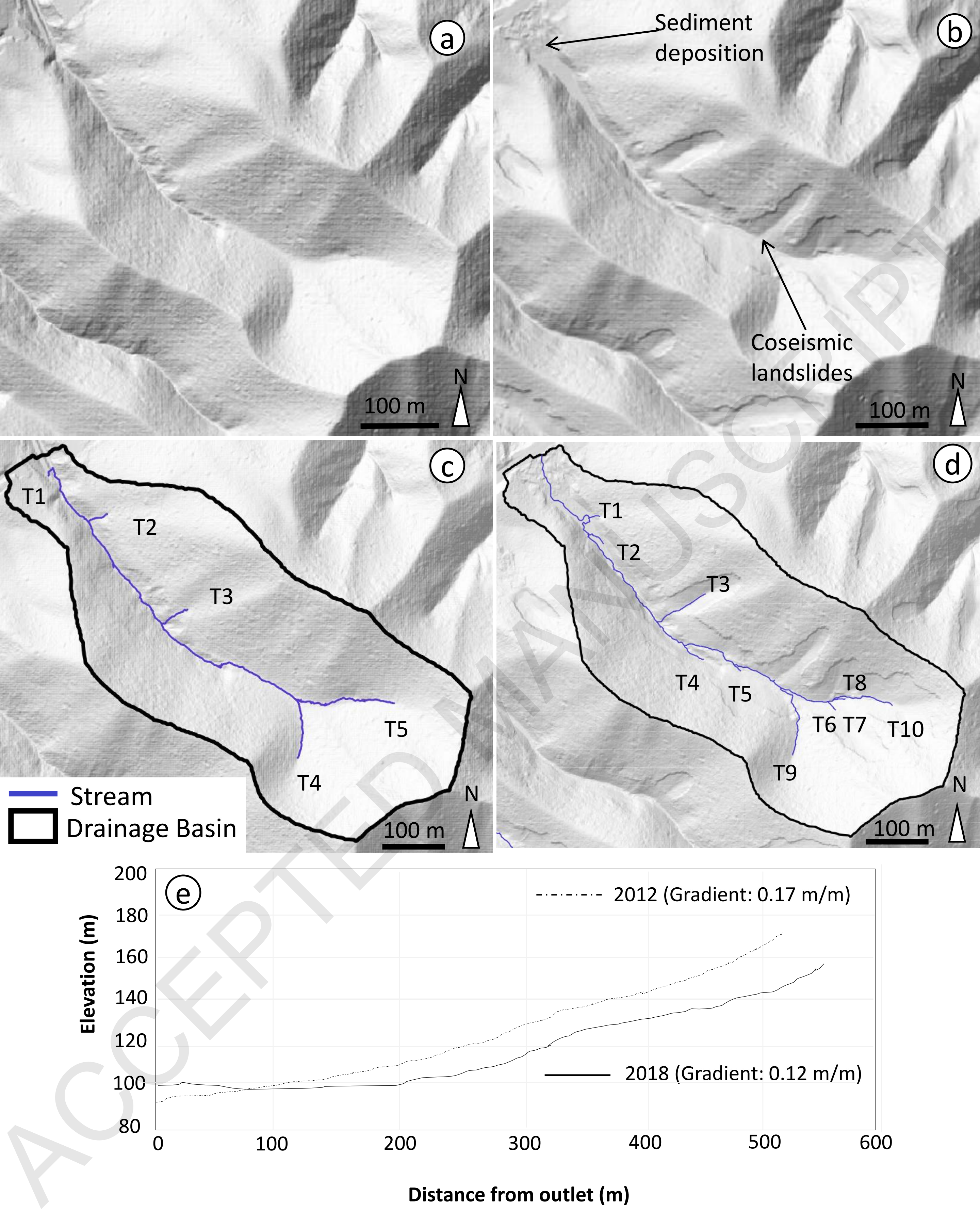

Figure 4. Pre- and post-earthquake morphological changes and drainage network development in Period 1. (a) Hillshade image of ALS DEM in October 2012. (b) Hillshade image of ALS DEM in September 2018 after the earthquake. (c) Stream network delineated from the pre-earthquake ALS DEM in 2012. (d) Stream network delineated from the post-earthquake ALS DEM in 2018. (e) Longitudinal profile of the mainstream in 2012 (red) and 2018 (gray). Note that the horizontal distance along the channel is elongated for the channel in 2018 because of the more meandered channel shape.

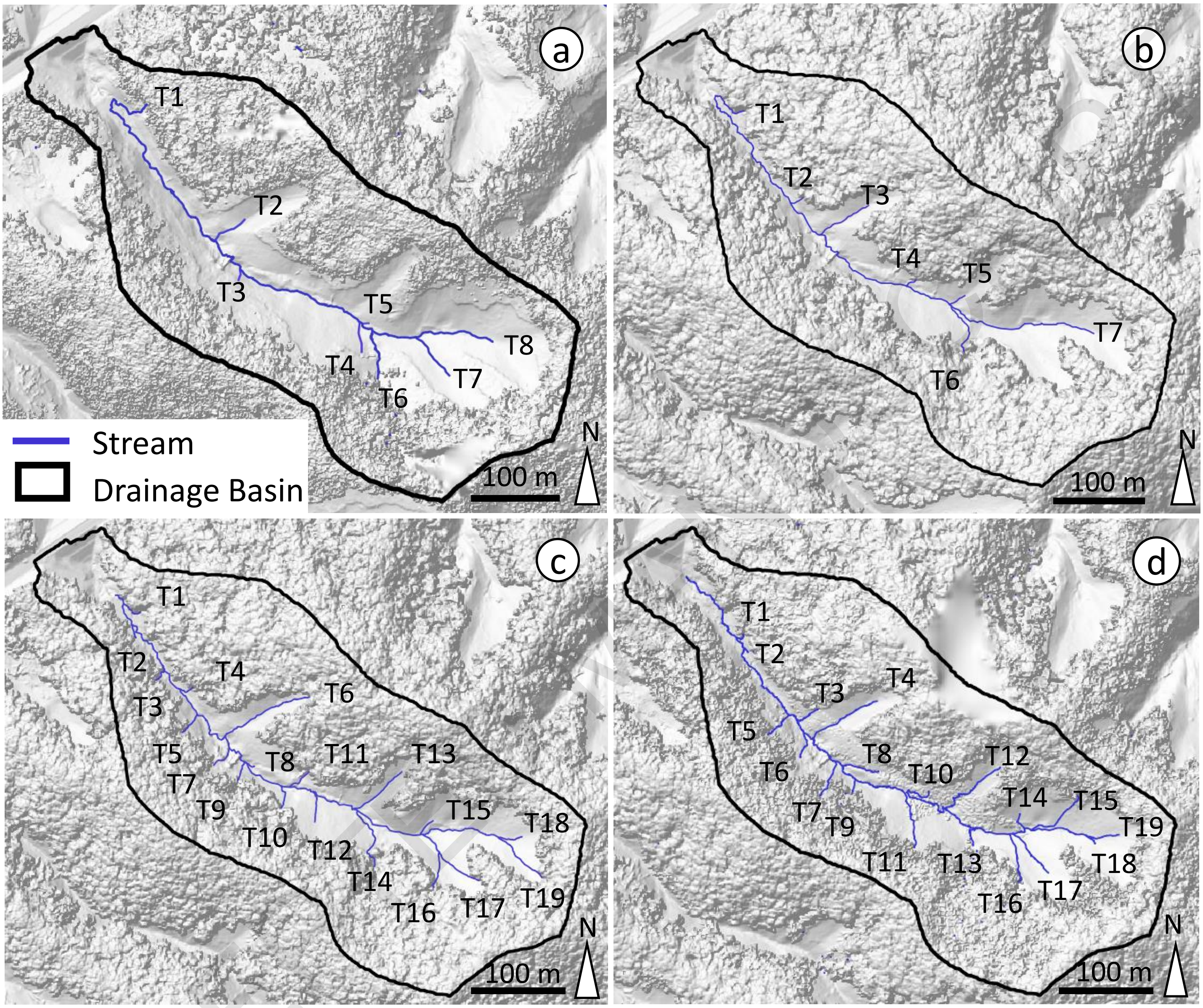

Figure 5. Post-earthquake morphological characteristics and drainage network development in 2020 (Periods 2-5). Hillshade image and stream network for (a) April 23, (b) June 25, (c) September 14, and (d) October 30.

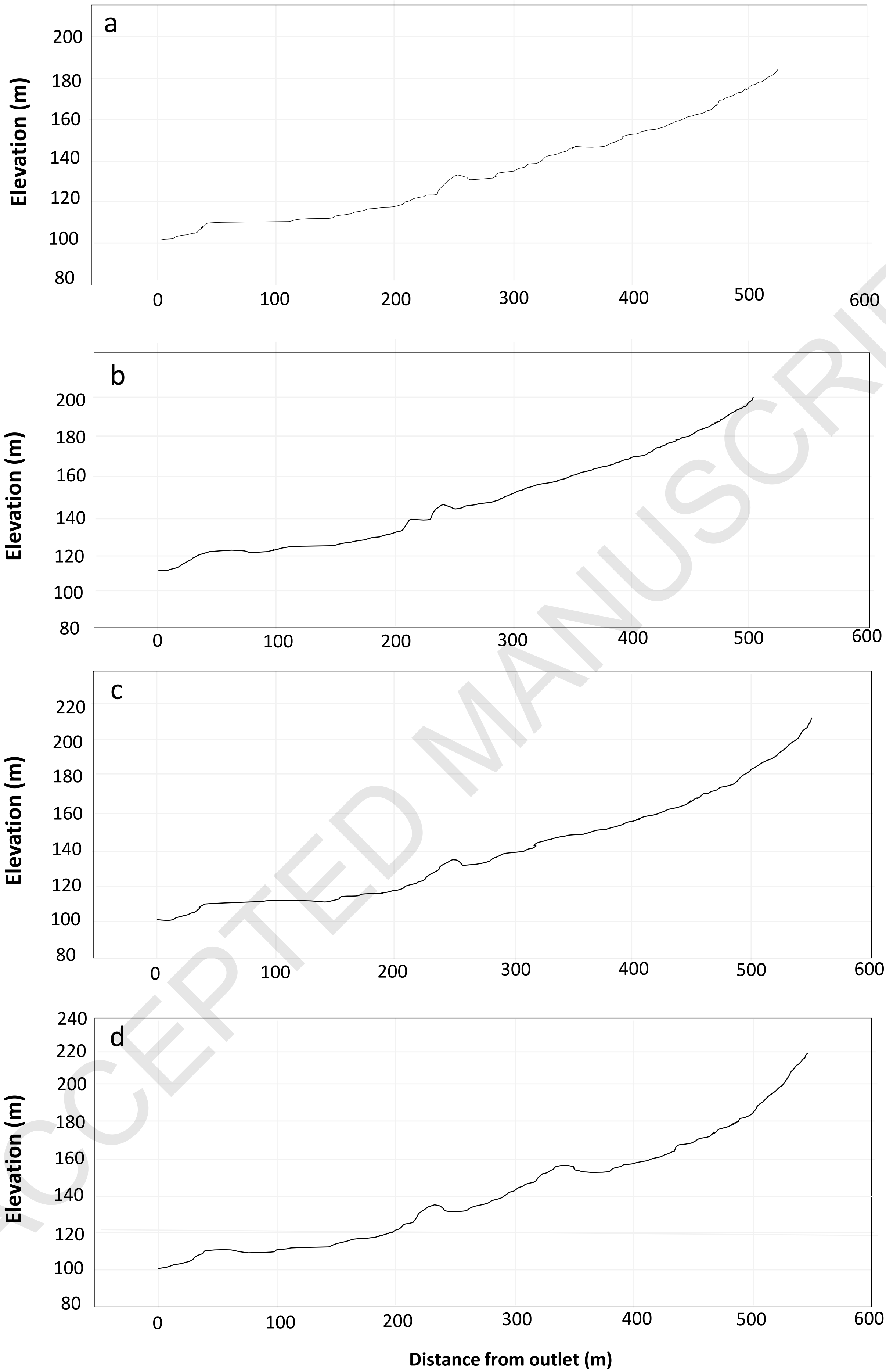

Figure 6. Longitudinal profiles of mainstream for each time of measurement by UAV-based SfM-MVS photogrammetry. (a) April 2020. (b) June 2020. (c) September 2020. (d) October 2020.

Figure 7. Photograph of frost heave in study site taken on 31st March 2023. Height of frost heave was about 9 cm.

Table 1. Properties of topographic data used.

Period	Period 1	Period 2	Period 3	Period 4	Period 5	
Duration (months)	72	20	2	3	2	
Date	Oct 05, 2012	Sep 11, 2018	Apr 23, 2020	Jun 25, 2020	Sep 14, 2020	Oct 30, 2020
Type of acquisition	ALS	ALS	UAV	UAV	UAV	UAV
Reolution of DEM (m)	0.5	0.5	0.115	0.112	0.062	0.073

Table 2. Geomorphometric parameters of drainage basin characteristics examined in this study.

Types	Morphometric parameters	Unit	References	Equations
Drainage network	Stream number (N_u)	–	(Horton 1945)	$Nu = N_1 + N_2 + ...N_n$
	Stream length (L_u) (m)	m	(Horton 1945; Strahler 1964)	$Lu = L_1 + L_2 + ...L_n$
	Bifurcation ratio (R_b)	–	(Horton 1945; Strahler 1964)	$R_b = N_u / N_{u+1}$
	Mean gradient of mainstream	m/m		$(E\max - E\min) / Lm$
Drainage texture	Drainage density (D_d)	m/m^2	(Horton 1945)	$D_d = L_u / A$
	Drainage intensity (D_i)	1/km	(Faniran 1968)	$D_i = F_s / D_d$
	Infiltration number (I_f)	–	(Faniran 1968)	$I_f = F_s \text{ x } D_d$
	Length of overland flow (L_o)	km	(Horton 1945)	$L_o = 1/(2D_d)$
	Constant of channel maintenance (C)	km^2/km	(Schumm 1956)	$C = 1/D_d$
Relief characteristics	Ruggedness number (R_n)	km/km^2	(Strahler 1964)	$R_n = H \text{ x } D_d$

*A** is basin area (km^2), *E*max and *E*min* are maximum/minimum elevation (m) of the mainstream, F_s* is stream frequency (N_u/A)($1/km^2$), *H** is total basin relief (m) (elevation between height of basin outlet and maximum height of basin), *L*m* is the horizontal length (m) along the mainstream,

Table 3. Temporal changes in morphometric parameters examined.

Types	Morphometric parameters	Stream (Drainage Basin area: 104006 m^2(0.104006 km^2) (11th September, 2018)					
		Oct 05, 2012	Sep 11, 2018	Apr 23, 2020	Jun 25, 2020	Sep 14, 2020	Oct 30, 2020
Drainage network	Stream number (N_u)	6	11	9	8	22	20
	Stream length (L_u) (m)	721.3	932.9	753.9	694.3	1121.9	1199.6
	Bifurcation ratio (R_b)	5 (1st order: 5, 2nd order: 1)	10 (1st order: 10, 2nd order: 1)	8 (1st order: 8, 2nd order: 1)	7 (1st order: 7, 2nd order: 1)	9.5 (1st order: 19, 2nd order: 2) 2 (2nd order:2, 3rd order: 1)	19 (1st order: 19, 2nd order: 1)
	Mean gradient of mainstream (m/m)	0.17	0.12	0.15	0.17	0.21	0.14
Drainage texture	Drainage density (D_d) (km/km^2)	6.94	8.97	7.25	6.68	10.79	11.53
	Drainage intensity (D_i) (1/km)	8.32	11.79	11.94	11.52	19.61	16.67
	Infiltration number (I_f)	400.57	948.69	627.21	513.45	2281.67	2217.92
	Length of overland flow (L_o) (km)	0.07	0.06	0.07	0.07	0.05	0.04
	Constant of channel maintenance (C) (km^2/km)	0.14	0.11	0.14	0.15	0.09	0.09
Relief characteristics	Ruggedness number (R_n) (km/km^2)	1.18	1.63	1.15	1.06	1.71	1.81